

# Monte Carlo study of kink effect in isolated-gate InAs/AlSb high electron mobility transistors

B. G. Vasallo,<sup>1,a)</sup> H. Rodilla,<sup>1</sup> T. González,<sup>1</sup> G. Moschetti,<sup>2</sup> J. Grahn,<sup>2</sup> and J. Mateos<sup>1</sup>

<sup>1</sup>*Dpto. de Física Aplicada, Universidad de Salamanca, Plaza de la Merced s/n, 37008 Salamanca, Spain*

<sup>2</sup>*Department of Microtechnology and Nanoscience–MC2, Chalmers University of Technology, SE-412 96 Göteborg, Sweden*

(Received 16 July 2010; accepted 16 September 2010; published online 3 November 2010)

A semiclassical two-dimensional ensemble Monte Carlo simulator is used to perform a physical analysis of the kink effect in InAs/AlSb high electron mobility transistors (HEMTs). Kink effect, this is, an anomalous increase in the drain current  $I_D$  when increasing the drain-to-source voltage  $V_{DS}$ , leads to a reduction in the gain and a rise in the level of noise, thus limiting the utility of these devices for microwave applications. Due to the small band gap of InAs, InAs/AlSb HEMTs are very susceptible to suffer from impact ionization processes, with the subsequent hole transport through the structure, both implicated in the kink effect. The results indicate that, when  $V_{DS}$  is high enough for the onset of impact ionization, holes thus generated tend to pile up in the buffer (at the gate-drain side) due to the valence-band energy barrier between the buffer and the channel. Due to this accumulation of positive charge the channel is further opened and  $I_D$  increases, leading to the kink effect in the  $I$ - $V$  characteristics and eventually to the device electrical breakdown. The understanding of this phenomenon provides useful information for the development of kink-effect-free InAs/AlSb HEMTs. © 2010 American Institute of Physics.

[doi:[10.1063/1.3503430](https://doi.org/10.1063/1.3503430)]

## I. INTRODUCTION

Sb-based heterostructures, based on narrow band-gap semiconductors, in particular AlSb/InAs, are being considered to further improve the performance of high electron mobility transistors (HEMTs) for low-power, high-frequency, and low-noise applications.<sup>1–5</sup> However, these devices present some problems, in particular as the kink effect in the output current-voltage characteristics, caused by impact ionization and the subsequent hole dynamics in the heterostructure. In order to decrease the associated excessive gate leakage current, the conventional Schottky contact has been replaced by an insulated gate (by means of a native oxide, which naturally appears after the recess etch step<sup>6</sup>). However, impact ionization is still significant, and a study of the involved physical effects is essential to further optimize the structure design and thus further reduce the negative consequences of kink effect.

The aim of this work is to perform a physical analysis of the kink effect in recessed isolated-gate AlSb/InAs HEMTs. Charge carrier dynamics in these devices have been monitored by means of a semiclassical two-dimensional (2D) ensemble Monte Carlo (MC) simulator<sup>7,8</sup> adequately adapted to correctly model AlSb/InAs heterostructures,<sup>9</sup> in which both impact ionization and hole transport are included.<sup>10,11</sup> The validity of this model has been checked by comparing the extrinsic output characteristics with experimental results. MC method has been proved to be a very useful tool when dealing with problems where the understanding of the microscopic behavior of carriers is essential, as occurs when analyzing kink effect phenomena.<sup>10,11</sup> Moreover, the MC tech-

nique becomes the most adequate simulation tool since electron transport can easily turn into ballistic or at least quasiballistic in the channel of the analyzed transistors, because of the very high mobility of InAs.<sup>9</sup> The MC approach allows us to determine the origin and magnitude of the kink effect in terms of internal quantities, such as electron and hole concentrations and electric field profile. Hence a complete physical understanding of the kink phenomenon in these devices is achieved, providing helpful information for the development of kink-free Sb-HEMTs.

The paper is organized as follows. In Sec. II, the physical model is detailed. The main results of our simulations and their discussion are provided in Sec. III. Finally, in Sec. IV, we draw the most important conclusions of this work.

## II. PHYSICAL MODEL

For the device calculations, we make use of an ensemble MC simulator self-consistently coupled with a 2D Poisson solver which incorporates all the processes at the origin of the kink effect (impact ionization and hole dynamics). The simulated structure is very similar to the experimental one described in Ref. 5, what will be used to calibrate our model by reproducing the static characteristics. The source region, which is essentially ohmic, has been shortened in the simulated device in order to save computer time, its effect introduced as a resistance in a postprocessing stage. The structure under analysis is a 225 nm T-gate recessed HEMT [Fig. 1(a)], fabricated on a heterostructure consisting of a InP substrate (not simulated), a 800 nm AlSb buffer followed by a 15 nm thick InAs channel, two layers of AlSb (a 5 nm spacer and a 10 nm Schottky layer, separated by a  $5 \times 10^{12} \text{ cm}^{-2}$   $\delta$ -doped layer), and, finally, a 4 nm thick AlInAs and 5 nm

<sup>a)</sup>Electronic mail: [bgvasallo@usal.es](mailto:bgvasallo@usal.es).

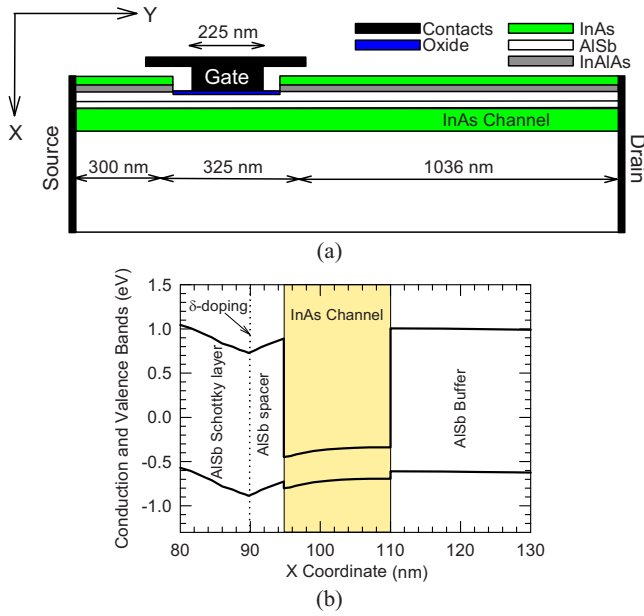


FIG. 1. (Color online) (a) Schematic drawing of the HEMT topology used in the simulations. (b) Conduction and valence bands for the AlSb/InAs heterostructure under analysis.

thick InAs cap layer ( $N_D = 5 \times 10^{18} \text{ cm}^{-3}$ ). The MC parameters for the electron transport simulation in the involved materials can be found in Ref. 9. Figure 1(b) presents the conduction and valence bands provided by the MC simulations for the AlSb/InAs heterostructure.

Impact ionization of electrons, which occurs in the  $\Gamma$  valley of InAs and leads to the appearance of holes, is included in the MC simulations by using the Keldysh approach,<sup>12</sup> where the probability per unit time of having an impact ionization event is given by  $P(E) = S[(E - E_{th})/E_{th}]^2$  if  $E > E_{th}$ , and  $P(E) = 0$  if  $E < E_{th}$ ,  $E$  being the electron kinetic energy in the  $\Gamma$  valley,  $E_{th}$  the ionization threshold energy and  $S$  a measure of the softness or hardness of the threshold.  $E_{th}$  and  $S$  are considered as adjustable parameters to reproduce the ionization coefficient (number of impact ionization events that occur per unit length) measured in bulk materials. From each impact ionization occurrence, an electron in the  $\Gamma$  valley and a hole in the heavy-hole (HH) band emerge, while the electron originating the ionization process remains in the  $\Gamma$  valley. We have verified, by analyzing the hole dynamics in InAs with the MC approach, that hole impact ionization is negligible for the considered applied voltages. Figure 2 presents, for InAs (channel material), the simulated values of (a) the electron velocity with and without considering impact ionization in the simulations as a function of the electric field, and (b) the impact ionization coefficient for  $E_{th} = 0.41 \text{ eV}$  and  $S = 10^{12} \text{ s}^{-1}$  as a function of the inverse of the electric field in comparison with the results obtained in Refs. 12 and 13. For these values of  $E_{th}$  and  $S$ , a remarkable agreement with other numerical estimations of the impact ionization coefficient is achieved. According to Fig. 2(a), when impact ionization is considered, the electron peak velocity is higher than in the case of neglecting impact ionization processes. This occurs because the onset of impact ionization takes place for electron energies lower than those necessary

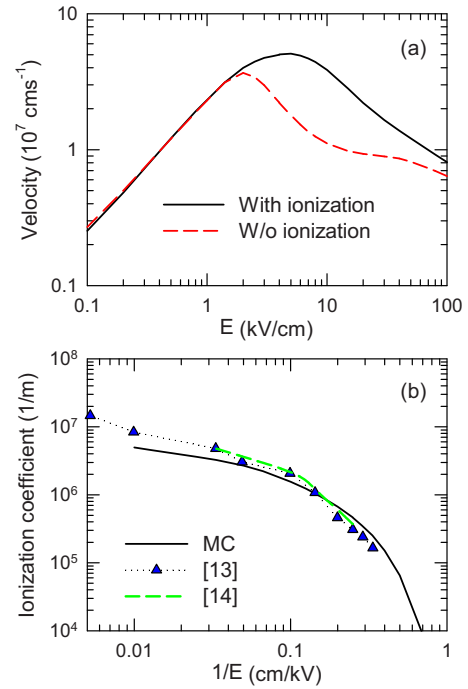


FIG. 2. (Color online) MC values in bulk InAs of (a) the electron velocity in both cases with and without considering impact ionization vs electric field and (b) impact ionization coefficient vs inverse of electric field in comparison with the values in Refs. 12 and 13.  $E_{th} = 0.41 \text{ eV}$ ,  $S = 10^{12} \text{ s}^{-1}$ .

for intervalley transfer (otherwise very frequent in bulk InAs), so that the electron occupancy in the  $\Gamma$  valley is higher than in the absence of impact ionization. As a consequence, the maximum electron velocity increases and takes place for a higher electric field.<sup>9</sup> The calculated low-electric field mobility is about  $28\,000 \text{ cm}^2/\text{V s}$ , within the experimental range.<sup>14</sup>

With respect to the model used for hole dynamics, a typical spherical and nonparabolic valence-band structure is considered, including three sub-bands: HH and light-hole bands (HH and LH), degenerated at  $\mathbf{k} = 0$  and characterized by a different curvature in  $\mathbf{k}$ -space, and a third split-off band (SOH), in which the band warping is accounted for by the use of approximated overlap functions.<sup>15</sup> Ionized impurity, acoustic, polar, and nonpolar optical phonon scattering mechanisms are considered for holes.<sup>15,16</sup> The hole physical parameters used in the simulations are reported in Table I, providing a low-electric-field mobility of  $350 \text{ cm}^2/\text{V s}$  for InAs and  $525 \text{ cm}^2/\text{V s}$  for AlSb, both within the respective experimental ranges.<sup>14</sup>

Another important process that is necessary to take into account for a proper analysis of kink effect is hole recombination.<sup>10</sup> To this end we used a simple model in which hole recombination is considered to take place with a characteristic time  $\tau_{rec}$  (i.e., with a probability  $1/\tau_{rec}$ ). We performed simulations with  $\tau_{rec} = 0.05 \text{ ns}$  (even if in bulk materials it is usually considered to be of the order of  $1 \text{ ns}$ ), since with this value together with those of  $E_{th}$  and  $S$  adequately reproduce the experimental static  $I$ - $V$  characteristics are adequately reproduced, as we will show in Sec. III.

TABLE I. Physical parameters of holes in InAs and AISb.

Parameter	InAs			AISb		
	HH	LH	SOH	HH	LH	SOH
Band gap (eV)	0.354			0.6035	0.1070	0.2200
Optical phonon energy (eV)	0.03			1.0	0.9	0.8
Optical deformation potential (eV/m)	11.3			0.0	0.0	0.973
Acoustic deformation potential (eV)	20.0					
Effective mass ( $m^*/m_0$ )	0.570	0.025	0.140	0.6035	0.1070	0.2200
Nonparabolicity (1/eV)	1.0	0.9	0.8	1.0	0.9	0.8
Energy level from HH (eV)	0.0	0.0	0.39	0.0	0.0	0.973

### III. RESULTS

Figure 3 shows the simulated (a) extrinsic and (b) intrinsic output  $I$ - $V$  characteristics of the InAs/AISb HEMT with and without impact ionization. The experimental  $I$ - $V$  curves taken from Ref. 5 have been included in Fig. 3(a) for comparison. In order to carry out the comparison of the measured results (extrinsic) with those obtained from the simulation (intrinsic), it is necessary to include, in a postprocessing stage, the parasitic elements that are not considered in the intrinsic MC model.<sup>17</sup> Thus, drain and source parasitic resistances associated with contact metallization and part of the ohmic regions not included in the simulation domain have been incorporated into the original MC results, with the best fit being obtained for  $R_S=0.13 \ \Omega \text{ mm}$  and  $R_D=0.38 \ \Omega \text{ mm}$ .

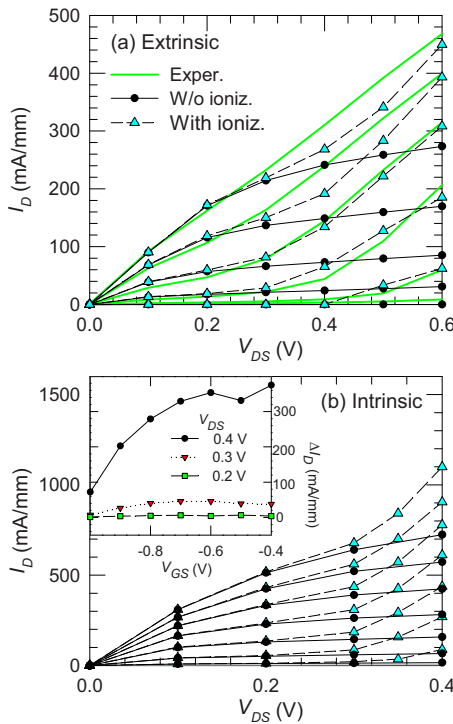


FIG. 3. (Color online) MC (a) extrinsic and (b) intrinsic output characteristics for the InAs/AISb HEMT in presence and absence of impact ionization, being  $E_{th}=0.41 \text{ eV}$ ,  $S=10^{12} \text{ s}^{-1}$ , and  $\tau_{rec}=0.05 \text{ ns}$ . Experimental results of the similar fabricated structure are plotted in (a) for comparison.  $V_{GS}$  is  $-0.45 \text{ V}$  in (a) and  $-0.40 \text{ V}$  in (b) for the top curves, and the potential step is  $\Delta V_{GS}=-0.1 \text{ V}$ . Inset: difference of  $I_D$  with and without considering impact ionization vs  $V_{GS}$  for different  $V_{DS}$ .

An excellent agreement between experimental and simulated results is reached [Fig. 3(a)] when considering impact ionization in the simulations with values for the involved parameters of  $E_{th}=0.41 \text{ eV}$ ,  $S=10^{12} \text{ s}^{-1}$ , and  $\tau_{rec}=0.05 \text{ ns}$ , as mentioned previously. A notable increase in  $I_D$  takes place starting from a value of  $V_{DS}$  high enough so that the electron energy is sufficient for the onset of impact ionization. On the contrary, in the absence of impact ionization the output curves are fitted just up to  $V_{DS}=0.2 \text{ V}$ . In the inset of Fig. 3(b), the difference in the values of  $I_D$  obtained with and without considering impact ionization is plotted as a function of  $V_{GS}$  for different values of  $V_{DS}$ . The increase in  $I_D$  for a fixed  $V_{DS}$  due to the appearance of holes grows with  $V_{GS}$ . This behavior is the opposite of that found for lattice-matched InGaAs/InAlAs HEMTs, in which the increase in  $I_D$  is lower for higher  $V_{GS}$ . This occurs because although the electron concentration in the channel is larger when the channel opens, the maximum electron energy is reduced due to the lower gate-to-drain potential.<sup>10,11</sup> In the case of InAs/AISb HEMTs, the band gap of the channel material is much smaller than in InGaAs/InAlAs HEMTs, so that the threshold energy  $E_{th}$  is also smaller. Thus impact ionization probability still remains significant for higher values of  $V_{GS}$ . Furthermore, impact ionization events occur not only near the maximum of electron energy (under the gate electrode), but all along the drain side of the channel, where the electron velocity is higher when increasing  $V_{GS}$  (to be shown below).

The isolated gate reduces the gate leakage current, but in the experimental device  $I_G$  still shows the typical bell-shape due to the outflow of holes, signature of impact ionization in standard Schottky-Gate field-effect transistors.<sup>6</sup>  $I_G$  is zero in the ideal simulated structures, since the gate current due to hole tunneling is not considered in our model.

MC simulations provide an insight into the kink effect for InAs/AISb HEMTs. Initially, the influence of  $V_{GS}$  will be analyzed. Figure 4 shows the profiles along the InAs channel of: (a) the number of impact ionization events taking place in the channel, (b) the sheet hole density in the buffer and the cap layer, (c) the sheet electron density, and (d) mean electron velocity in the channel, for  $V_{DS}=0.4 \text{ V}$  and different values of  $V_{GS}$ . As observed in Fig. 4(a), the impact ionization events take place in the drain side of the channel, mainly close to the drain side of the recess, where the electric field, and consequently the electron energy, is higher. In fact, the kink effect is commonly avoided (actually shifted to higher

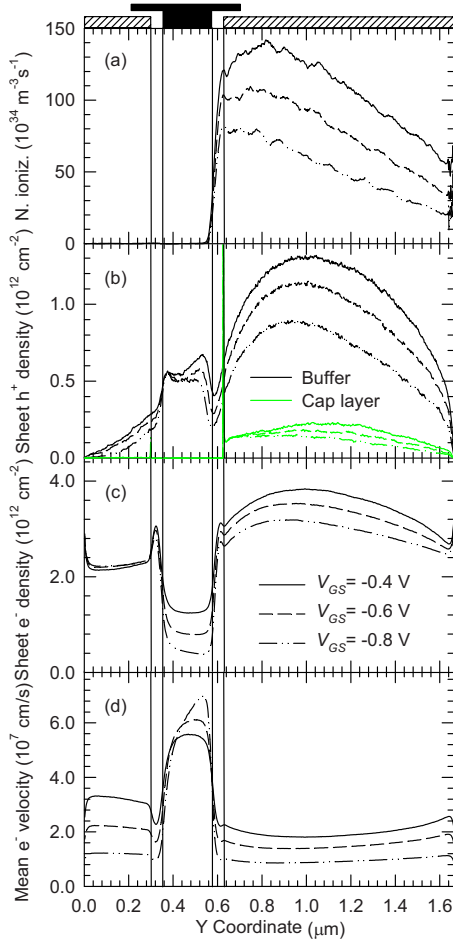


FIG. 4. (Color online) Profiles along the channel of: (a) impact ionization events in the channel per unit time and depth, (b) hole sheet density in the buffer and the cap layer, (c) sheet electron density, and (d) mean electron velocity in the channel for different values of  $V_{GS}$ , being  $V_{DS}=0.4$  V,  $E_{th}=0.41$  eV,  $S=10^{12}$  s $^{-1}$ , and  $\tau_{rec}=0.05$  ns. The position of the gate and the recess is also indicated.

biases) by enlarging the drain recess length, which leads to a lower electric field in that region. Moreover, the few impact ionization events taking place in the InAs cap layer lead to a concentration of holes moving toward the gate electrode and piling up in the gate side of the cap layer [Fig. 4(b)], where they disappear by recombination.

Even if a few holes generated by impact ionization in the drain side of the channel move toward the AISb spacer, most of them, due to the vertical electric field, descend the energy step present in the valence band at the heterojunction between the InAs channel and the AISb buffer [Fig. 1(b)]. Once there, their energy decreases because of scattering mechanisms, and holes are no longer able to surmount the energy barrier in the valence band preventing their return back to the channel. Thus holes accumulate in the buffer, mainly at the drain side and under the gate [Fig. 4(b)]. Almost none of them arrive to the source electrode because they recombine before reaching the source side of the buffer. The increase in  $I_D$  can be mostly explained as a consequence of this pileup of positive charge, which lowers the potential barrier that controls the current through the channel. As a result, the channel is further opened and the electron density (and drain current  $I_D$ ) increases [Fig. 4(c)]. The rise of  $I_D$  is basically due to this

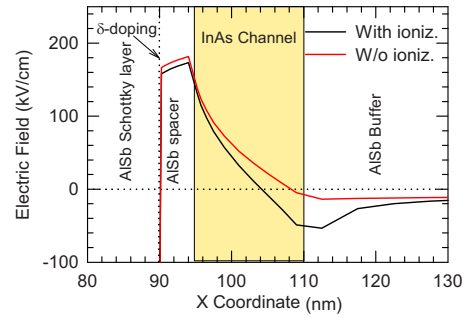


FIG. 5. (Color online) Vertical electric field profile along the x-direction under the source side of the recess in presence and absence of impact ionization for  $V_{DS}=0.4$  V,  $V_{GS}=-0.6$  V,  $E_{th}=0.41$  eV,  $S=10^{12}$  s $^{-1}$ , and  $\tau_{rec}=0.05$  ns. The position of the different active layers is also indicated.

enhancement in the electron flow through the channel, since the number of electrons/holes generated by impact ionization is very low so as to provide a significant contribution to  $I_D$ . Moreover, the mean value of the electron velocity [Fig. 4(d)] is higher at the drain side of the channel for higher values of  $V_{GS}$ , which contributes also to the enhancement of  $I_D$ . Notice that both electron concentration and mean velocity are higher at the drain side of the channel for increasing values of  $V_{GS}$  while at the source side the electron density is similar, which leads to larger differences in the mean velocity.

The effect of the pileup of holes in the buffer can be observed in the behavior of the vertical electric field. In Fig. 5, the vertical electric field under the source side of the recess is represented along the vertical direction with and without impact ionization, for a bias of  $V_{DS}=0.4$  V and  $V_{GS}=-0.6$  V. When the hole accumulation is not present in the structure, the electric field in the channel takes positive values; then, electrons tend to move up and flow through the upper part of the channel. The presence of the hole pileup leads to a reduction in the energy barrier present at the source side of the gate that limits the entrance of electrons into the active region of the transistor, thus allowing for more electrons to flow through the device. Additionally, it originates a negative vertical electric field near the buffer, so that most of the excess electrons flow through the bottom part of the channel.

To further illustrate this effect, Fig. 6 presents the contour maps of (a) the difference between the electron concentration with and without considering impact ionization, and (b) hole concentration, for a bias of  $V_{DS}=0.4$  V and  $V_{GS}=-0.6$  V. Since the hole pileup takes place in the buffer, the difference in electron concentration under the gate between the two cases is higher at the bottom than at the top part of the channel. However, the most important increase in electron concentration appears at the drain side of the channel, thus further increasing the drain conductance of the transistor, and the kink observed in the  $I$ - $V$  curves.

## IV. CONCLUSIONS

We have presented a microscopic analysis of kink effect in insulated-gate recessed AISb/InAs HEMTs based on MC simulations. The results allow interpreting the effect in terms of the pileup of holes (generated by impact ionization at the

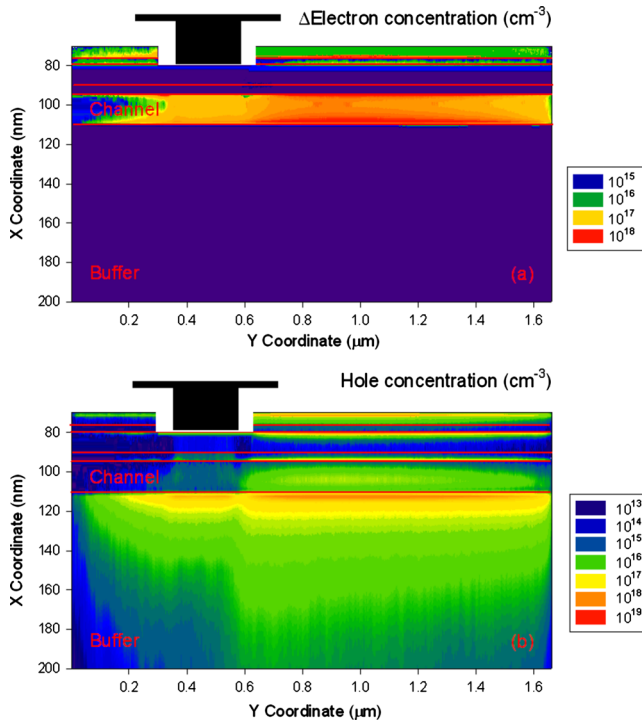


FIG. 6. (Color online) Contour maps of (a) the difference between the electron concentration with and without considering impact ionization, and (b) hole concentration, for  $V_{DS}=0.4$  V,  $V_{GS}=-0.6$  V,  $E_{th}=0.41$  eV,  $S=10^{12}$  s $^{-1}$ , and  $\tau_{rec}=0.05$  ns. The position of the gate and the recess is also indicated.

drain region of the channel) at the drain-gate side of the buffer. This hole pileup takes place in the buffer because of the energy barrier in the valence band at the heterostructure between the AlSb buffer and the InAs channel. The positive charge due to the accumulation of holes contributes to further open the channel below the gate, mainly through its bottom side thus increasing the electron concentration in the active part of the device. Moreover, impact ionization produces an important enhancement of the electron concentra-

tion at the drain side of the channel, leading to a further increase in the drain conductance and the kink effect in the  $I$ - $V$  curves.

## ACKNOWLEDGMENTS

This work has been partially supported by the European Commission through the ROOTHz Project ICT-2009-243845 and the MC2ACCESS Project, by the Dirección General de Investigación (MEC) and FEDER through Project TEC2007-61259/MIC and by the Consejería de Educación, Junta de Castilla y León through Projects SA019A08 and GR270.

- <sup>1</sup>C. R. Bolognesi, M. W. Dvorak, and D. H. Chow, *IEEE Trans. Electron Devices* **46**, 826 (1999).
- <sup>2</sup>J. B. Hacker, J. Bergman, G. Nagy, G. Sullivan, C. Kadow, H. K. Lin, A. C. Gossard, M. Rodwell, and B. Brar, *IEEE MTT-S Int. Microwave Symp. Dig. 1-4*, 1029 (2005).
- <sup>3</sup>W. Kruppa, J. B. Boos, B. R. Bennett, N. A. Papanicolaou, D. Park, and Robert Bass, *IEEE Trans. Electron Devices* **54**, 1193 (2007).
- <sup>4</sup>C.-Y. Chang, H.-T. Hsu, E. Y. Chang, C.-I. Kuo, S. Datta, M. Radosavljevic, Y. Moyamoto, and G.-W. Huang, *IEEE Electron Device Lett.* **28**, 856 (2007).
- <sup>5</sup>M. Malmkvist, E. Lefebvre, M. Borg, L. Desplanque, X. Wallart, G. Dambriane, S. Bollaert, and J. Grahn, *IEEE Trans. Microwave Theory Tech.* **56**, 2685 (2008).
- <sup>6</sup>E. Lefebvre, M. Malmkvist, M. Borg, L. Desplanque, X. Wallart, G. Dambriane, S. Bollaert, and J. Grahn, *IEEE Trans. Electron Devices* **56**, 1904 (2009).
- <sup>7</sup>J. Mateos, T. González, D. Pardo, V. Hoel, H. Happy, and A. Cappy, *IEEE Trans. Electron Devices* **47**, 250 (2000).
- <sup>8</sup>J. Mateos, T. González, D. Pardo, V. Hoel, and A. Cappy, *Semicond. Sci. Technol.* **14**, 864 (1999).
- <sup>9</sup>H. Rodilla, T. González, D. Pardo, and J. Mateos, *J. Appl. Phys.* **105**, 113705 (2009).
- <sup>10</sup>B. G. Vasallo, J. Mateos, D. Pardo, and T. González, *J. Appl. Phys.* **94**, 4096 (2003).
- <sup>11</sup>B. G. Vasallo, J. Mateos, D. Pardo, and T. González, *J. Appl. Phys.* **95**, 8271 (2004).
- <sup>12</sup>M. V. Fischetti, *IEEE Trans. Electron Devices* **38**, 634 (1991).
- <sup>13</sup>K. Brennan and K. Hess, *Solid-State Electron.* **27**, 347 (1984).
- <sup>14</sup>O. Madelung, *Semiconductors: Data Handbook* (Springer, Berlin, 2004).
- <sup>15</sup>T. Brudevoll, T. A. Fjeldly, J. Baek, and M. S. Shur, *J. Appl. Phys.* **67**, 7373 (1990).
- <sup>16</sup>M. Costato and L. Reggiani, *Phys. Status Solidi B* **58**, 471 (1973).
- <sup>17</sup>S. Babiker, A. Asenov, N. Cameron, and S. P. Beaumont, *IEEE Trans. Electron Devices* **43**, 2032 (1996).